文章编号：1001-9014(2020)06-0704-05

DOI:10.11972/j.issn.1001-9014.2020.06.007

The study and application of D-band radiometer front-end

LIU Jun, HE Wei, QIAO Hai-Dong, YU Wei-Hua*, LYU Xin

(Beijing Key Laboratory of Millimeter Wave and Terahertz Technology, Beijing Institute of Technology, Beijing 100081, China)

Abstract: A D-band (110~170 GHz) direct detection radiometer front-end which consists of detector module, low noise amplifier module and standard gain horn antenna. The D-band detector is designed and fabricated based on zero-bias Schottky barrier diode HSCH-9161 and the measurement shows that the voltage sensitivity is larger than 400 mV/mW between 110~140 GHz, larger than 120 mV/mW in D-band and the maximal value reaches about 1 600 mV/mW@110 GHz. The D-band LNA module is packaged with self-designed MMIC and the module measurement shows the peak gain is 10.8 dB@139 GHz, the gain higher than 7.8 dB from 137 GHz to 144 GHz, the measured input return loss (S11) and output return loss (S22) are better than -5 dB and 8.5 dB in operating frequencies, respectively. Finally, the imaging experiments based on this front-end are carried out.

Key words: D-band, radiometer front-end, low noise amplifier (LNA), detector

PACS: 07.57.Kp

D波段辐射计前端的设计与应用

刘 军, 何 伟, 乔海东, 于伟华*, 吕 昕

(北京理工大学 毫米波与太赫兹技术北京市重点实验室,北京 100081)

摘要:设计了D波段直接检波式辐射计前端,主要包括D波段检波器模块、D波段低噪声放大器模块和D波段标准增益喇叭天线.基于商用零偏二极管HSCH-9161研制出D波段检波器,测试结果显示在D波段内,最高灵敏度接近1 600 mV/mW,当频率小于140 GHz时,灵敏度大于400 mV/mW,在大于140 GHz频段内,灵敏度优于120 mV/mW.基于自研D波段低噪声放大器芯片研制出D波段低噪放模块,测试结果显示最大增益为10.8 dB@139 GHz,在137~144 GHz频率范围内,增益大于7.8 dB,输入端回波损耗优于5 dB,输出端回波损耗优于8.5 dB.最终搭建D波段直接检波式辐射计前端进行成像实验验证.

关 键 词:D波段;辐射计前端;低噪声放大器;检波器

中图分类号:TN454 **文献标识码**:A

Introduction

The millimeter-wave covers the frequency from 30 GHz to 300 GHz with the properties of relatively small wavelength and low-loss propagation in different frequency windows[1-2]. The passive imaging systems at millimeter-wave frequencies have excellent potential for high-resolution detection without requiring electronic or mechanical switching or local oscillator (LO) signal distribution[3-4]. The radiometer is attractive for applications such as imaging systems, passive surveillance sensors, concealed weapon detection, high-speed wireless communication, atmospheric sensing and high-resolution imaging[5-10]. The atmospheric propagation window at 94, 140 and 220 GHz allow propagation through fog, dust, and clothing and, therefore, these frequencies are especially appealing for security screening and low-visibility navigation systems[1,11]. Nowadays W-band imaging systems have already available and commercial. Compared with W-band imaging systems, D-band systems have a high potential for better spatial resolution and more compact size[12].

A D-band direct detection radiometer front-end is designed and carried out imaging verification in this paper. The radiometer front-end is built on detector mod-

Received date: 2020-03-01, **revised date**: 2020-09-11 **收稿日期**:2020-03-01,**修回日期**:2020-09-11

Foundation items: Supported by National Natural Science Foundation of China (61771057)

Biography: LIU Jun (1989-), male, Shandong, China, Ph. D. Research area involves terahertz device, circuit and package for imaging
E-mail: lj_bit@163.com

* **Corresponding author**: E-mail: ywhbit@bit.edu.cn

ule, low noise amplifier module and standard gain horn antenna. The D-band detector module is designed and fabricated based on zero-bias Schottky barrier diode HSCH-9161 and the D-band low noise amplifier (LNA) module is packaged with self-designed InP-based LNA MMIC. Finally, imaging experiments is carried out based on this radiometer front-end and have a good result, which lay a solid foundation for the practical application of the terahertz radiometer.

1 Low noise amplifier module

For improving the sensitivity and achieving good signal-to-noise ratio (SNR), a low noise amplifier is an essential need of every radiometer system. The better that noise performance is the weaker signals can be received and analyzed which correlates directly with the sensitivity or range of imaging systems. Improving the noise performance of a receiver is main job of a LNA. The amplifier circuit has been manufactured using 100-nm gate length InP HEMT technology in Ref. 13. In this paper, the selected amplifier has been assembled in an E-plan split-block waveguide package. The package design mainly includes transitions from microstrip to rectangular waveguide. The outer dimensions of the block are 30 mm×20 mm×25 mm and the LNA chips and chip capacitors are attached to the block with conductive epoxy glue. Figure 1 shows the photograph of the split-block module with MMIC, waveguide to microstrip transitions.

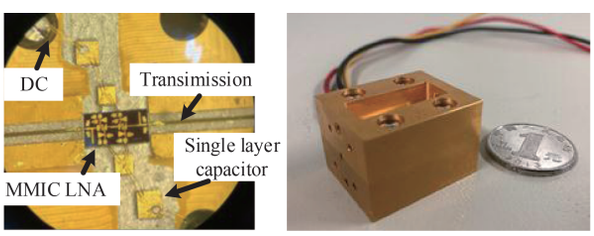

Fig. 1　(a) The split-block module with MMIC, (b) the photo of the LNA module
图1　(a)内部装配图, (b)低噪声放大器模块照片

The LNA module was measured using Rohde & Schwarz ZVA50 network analyzer with Rohde & Schwarz ZC170 (110~170 GHz) frequency extenders. The measurement results for the packaged LNA are shown in Fig. 2. The LNA module exhibits maximum gain of 10.8 dB at 145 GHz and 3 dB bandwidth is about 7 GHz from 137 GHz to 144 GHz. The measured input return loss S11 better than 5 dB and output return loss S22 better than 8.5 dB in the frequency from 125 GHz to 155 GHz. Due to the waveguide flange is not suitable, between the output port and test equipment have a split, the fluctuate of S22 is greatly with frequency. Another reason may be the wire-bonding at output port causes the matching performance changed. As shown in Fig. 2, the tendency of packaged S21 curve is same as the on-chip measured and its value is worse than the on-chip measurement about 5 dB. Due to the pad size is limited, a 25-μm bonding wire was used for connection is the main reason of the deterioration of the LNA module performance. The noise figure is about 5 dB and the DC power consumption is about 32.4 mW with a drain voltage of V_{ds}=1.2 V.

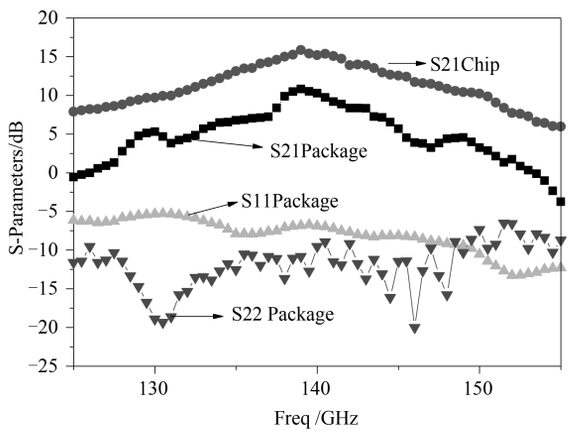

Fig. 2　LNA packaged measured S-parameters, on-chip S21
图2　LNA封装S参数与在片S21对比

2 Detector module

The millimeter wave detectors play an important role in many millimeter wave systems such as power detection devices, direct detection receivers and imaging system. With the development of millimeter wave technologies, there is pressing need of compact and highly sensitive detector that operated at room temperature. Schottky diodes with the properties of low parasitic capacitance and series resistance provides an efficient solution for millimeter wave detection under room temperature [14].

A D-band detector was designed based on zero-bias Schottky barrier diode HSCH-9161 and Fig. 3 shows the schematic diagram of the detector. Figure 4 shows small signal linear model of the HSCH-9161 that include junction resistance R_j, junction capacitance C_j, series resistance R_s, parasitic capacitance C_s and parasitic inductance L_s.

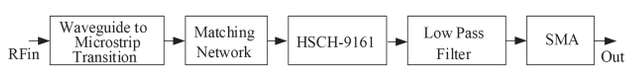

Fig. 3　Schematic diagram of D-band detector
图3　D波段检波器原理图

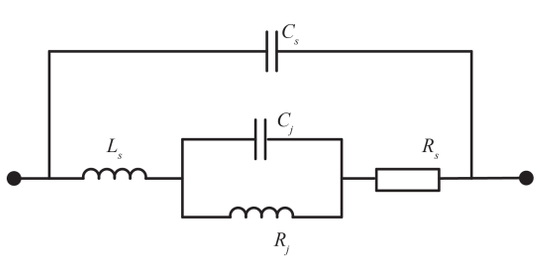

Fig. 4　Small signal linear model of HSCH-9161
图4　HSCH-9161小信号线性模型

All passive networks including waveguide to mi-

crostrip, matching network and low pass filter of the detectors are analyzed and designed by HFSS and fabricated on 50-μm quartz substrate. The simulation model and simulated result of input waveguide to microstrip transition is shown in Fig. 5. As shown in Fig. 5(b), the transmission loss below 0. 15 dB and the return loss above 20 dB from 118 to 172 GHz. For isolating the detector signal (DC or low frequency signal) from RF signal, a low pass filter (LPF) is designed as indicated in Fig. 6. From the simulated result of the LPF that presented in Fig. 6(b), the rejection above 20 dB in full D-band and the transmission loss is below 0. 15 dB in low frequency.

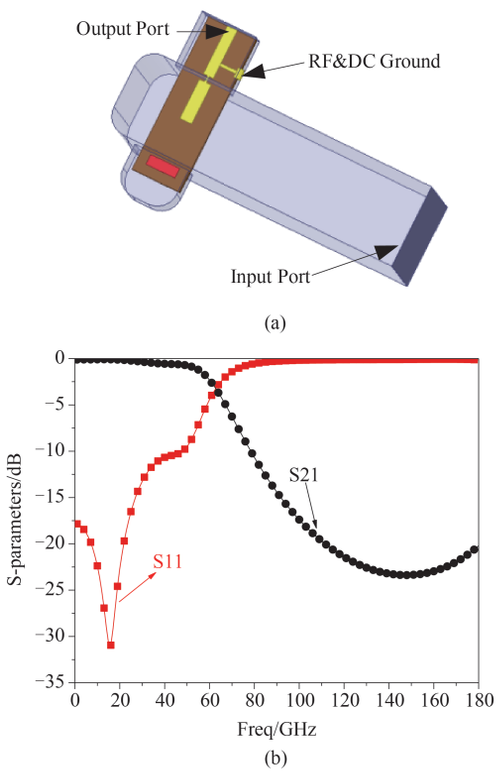

Fig. 5 (a) Simulation model of input waveguide to microstrip, and (b) the simulated result
图5 (a)输入波导-微带探针过渡仿真模型,(b)仿真结果

Finally, the quartz substrate was mounted to the waveguide block with conductive epoxy glue. The outer dimensions of the block are 20 mm×19 mm×15 mm and Fig. 7 shows the photo of the detector.

The diagram of voltage sensitivity measurement setup for the detector is shown in Fig. 8. A CETC-41 microwave source AV1464C with AV82406B (110~170 GHz) frequency extenders were employed to provide the D-band power, which was measured by Erickson power meter. An attenuator was adopted for ensuring the detector was operating in the square - law region that to keep the input power under -12 dBm. Finally, the output voltage was detected by digital multimeter.

The voltage sensitivity (R_v) of the detector can be calculated by

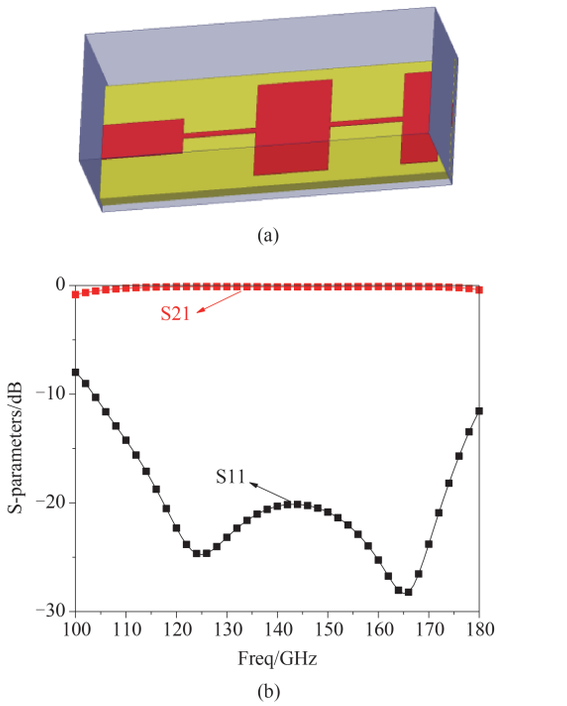

Fig. 6 (a)Simulation model of low pass filter, and (b) the simulated result
图6 (a)低通滤波器仿真模型,(b)仿真结果

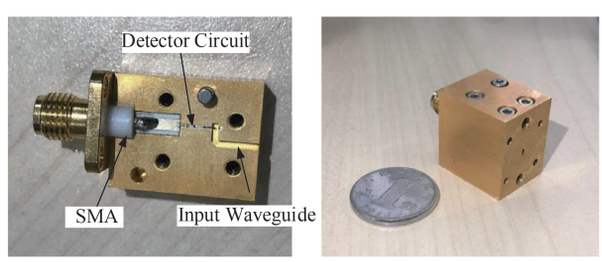

Fig. 7 Photo of the detector
图7 检波器实物图

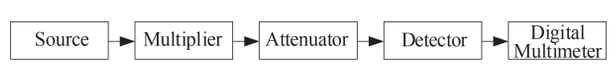

Fig. 8 Diagram of sensitivity measurement setup for detector
图8 检波器测试系统框图

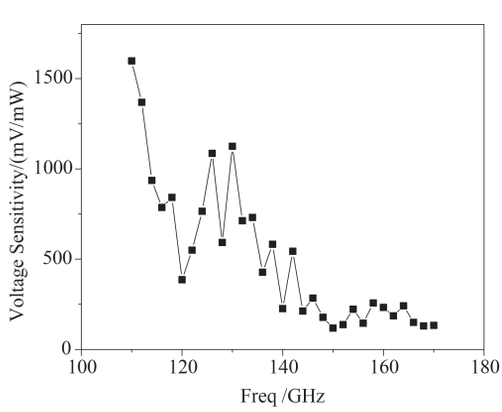

Fig. 9 The measured sensitivity of the detector
图9 检波器响应率测试图

$$R_v = \frac{V_{\text{out}}}{10^{P_{\text{in}}/10}} \quad , \quad (1)$$

where V_{out} is the voltage measured by digital multimeter and P_{in} is the incident RF power presented by Erickson power meter. The sensitivity of the detector is estimated by this method and the result is shown in Fig. 9. The measurement shows that the voltage sensitivity is larger than 400 mV/mW between 110~140 GHz, larger than 120 mV/mW in D-band and the maximal value reaches about 1600 mV/mW@110 GHz.

When the detector is working, the effective detection current mainly refers to the current through the junction resistance R_j. Due to the junction capacitance C_j and R_j are in parallel, it plays a certain bypass function, resulting in a decrease in sensitivity. Also, the series resistance R_s divides the valid voltage. The operate frequency f of the diode can be defined as

$$f = \frac{1}{2\pi C_j \sqrt{R_j R_s}} \quad . \quad (2)$$

As the frequency increases, the value of R_j decreases. Because the diode selected in this paper is suitable for W-band, as the frequency increases, the R_j will drop sharply, and the cut-off frequency is close to the D-band, so that most of the signal energy received by the diode is applied to R_s, which decreases R_j. The diode nonlinearity basically disappears, eventually causing its performance to be severely degraded.

3　Imaging experiments

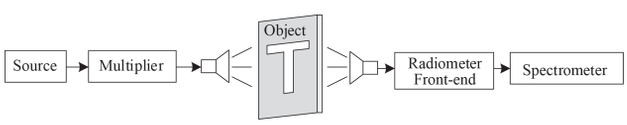

Fig. 10　Principle of imaging experimental
图 10　成像实验原理

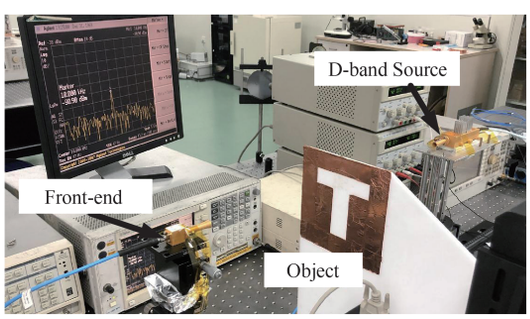

Fig. 11　Photo of the measurement setup
图 11　成像测试链路图

An imaging system that based on LNA module, detector module and standard horn antenna has been designed to demonstrate the imaging performance of our radiometer front-end. Based on the above module, the schematic diagram of imaging experiment and the measurement setup are shown in Figs. 10-11. As shown in Fig. 11, the imaging system is composed by D-band source, imaging object and the radiometer front-end. The D-band source is comprised by self-designed ×12 multiplication chains, providing a continuous output of 8mW at room temperature. The source is amplitude modulated with a modulation frequency of 10 kHz and an amplitude modulation depth of 100% and the RF signal is radiated through the standard horn antenna. The imaging object is a 15 cm×15 cm metal square with T shape hole, which moves with the 2D guide screw to achieve scanning. The receiving antenna is separated from the object by 15 cm, which means the resolution is 1.5 cm×1.5 cm. When transmitted through the T-shape area, the RF signal is detected by radiometer front-end and then read out by the spectrometer with a high potential, in other areas of the square structure, the signal is reflected and outputs low potential. The recorded potential in spectrometer will be numerically mapping to a grey scale for imaging.

First, we perform the imaging experiments only use detector and antenna and the imaging result is shown in Fig. 12. Compared with the real object, the Fig. 12 can clearly show the different characteristics of the T-shape and the outlines are basically same with the T-shape. At the same time, due to the metal edge cannot completely isolate the radiated signal, so some fuzzy points appeared in the T-shape edge area.

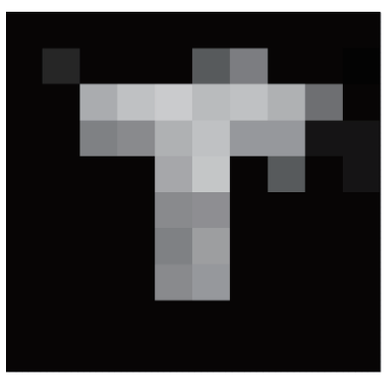

Fig. 12　Imaging result of the radiometer front-end without LNA
图 12　未加低噪声放大器的成像结果

Then the imaging experiments are performed with LNA module and detector module and the imaging result is shown in Fig. 13. Compared Fig. 12 with Fig. 13, after adding the LNA module to the front-end of the radiometer, there are still some edge blur points, increasing the signal reception intensity and detection output level, improving the signal-to-noise ratio. The contrast to the image is improved, and the imaging result is better.

The noise equivalent temperature difference (NETD) is an important figure of merit for determining radiometer sensitivity. NETD is related to the thermal responsibility of the system and can be defined using system parameters as

$$\text{NETD} = \frac{T_S + T_R}{\sqrt{B\tau}} \quad , \quad (3)$$

where τ is the integration time, B is the RF bandwidth,

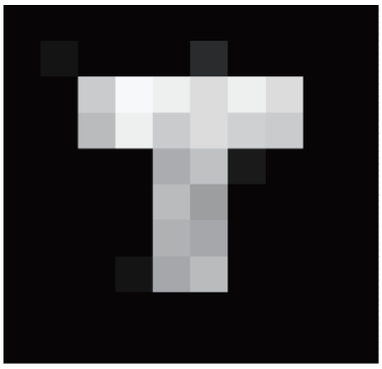

Fig. 13 Imaging result of the radiometer front-end with LNA
图13 加入低噪声放大器之后辐射计前端的成像结果

T_S is the scene temperature and T_R is the receiver noise temperature. Due to the bandwidth of LNA module is about 20 GHz, according to Eq. 3, when τ = 1 ms and B = 20 GHz, the ideal NETD of the system are estimated to be about 0.2 K. For better image quality, increasing the bandwidth and decreasing the noise figure of LNA and choosing a diode that suitable for D-band for improving the voltage sensitivity is necessary.

4 Conclusion

In this paper, a D-band direct detection radiometer front-end which consists detector module, low noise amplifier module and standard gain horn antenna is designed and the imaging experiments have been carried out. The D-band detector module is designed and fabricated based on zero-bias Schottky barrier diode HSCH-9161 and the D-band LNA module is packaged with self-designed InP-based LNA MMIC. The imaging experiments are carried out based on this radiometer front-end and the results are compared with or without LNA module. After adding the LNA module the contrast to the image is improved, and the imaging result is better. This radiometer front-end lays a solid foundation for the practical application of the terahertz radiometer.

References

[1] Kanar T, Rebeiz G M. A low-power 136-GHz SiGe total power radiometer with NETD of 0.25 K[J]. *IEEE Transactions on Microwave Theory & Techniques*, 2016, **64**(3): 906-914.

[2] Viegas C, Alderman B, Powell J, *et al*. Millimeter wave radiometers for applications in imaging and nondestructive testing[C]// Millimeter Waves & Thz Technology Workshop. IEEE, 2016.

[3] Gu Q J, Xu Z, Tang A, *et al*. A D-band passive imager in 65 nm CMOS[J]. *IEEE Microwave and Wireless Components Letters*, 2012, **22**(5): 263-265.

[4] Dacquay E, Tomkins A, Yau K H K, *et al*. D-band total power radiometer performance optimization in an SiGe HBT technology [J]. *IEEE Transactions on Microwave Theory & Techniques*, 2012, **60**(3): 813-826.

[5] Viegas C, Alderman B, Powell J, *et al*. Millimeter wave radiometers for applications in imaging and nondestructive testing[C]. Millimeter Waves & Thz Technology Workshop. IEEE, 2016.

[6] Dunne J, Mann C. Detection of corrosion under paints and insulating layers using passive millimetre wave imaging[C]. Active & Passive Rf Devices Seminar. IET, 2016.

[7] Ben Yishay R., Elad D. D-band Dicke-radiometer in 90 nm SiGe BiCMOS technology[C]. (2017) IEEE MTT-S International Microwave Symposium Digest, *art*. no. 8059046, pp. 1957-1960.

[8] Hassanin A I M, Shaaban A S E, Abd El-Samie F E. Medical applications of image reconstruction using electromagnetic field in terahertz frequency range[C]. 2019 International Symposium on Networks, Computers and Communications (ISNCC), Istanbul, Turkey, 2019, pp. 1-4.

[9] Skotnicki T, Knap W. Terahertz technologies and applications[C]. 2019 MIXDES - 26th International Conference "Mixed Design of Integrated Circuits and Systems", Rzeszów, Poland, 2019, pp. 34-37.

[10] AlNabooda M O, Shubair R M, Rishani N R, *et al*. Terahertz spectroscopy and imaging for the detection and identification of Illicit drugs[C]. 2017 Sensors Networks Smart and Emerging Technologies (SENSET), Beirut, 2017, pp. 1-4.

[11] Aguilar E, Hagelauer A, Weigel R. A 155 GHz low-power total power radiometer in a 130 nm SiGe technology[C]. 2018 11th German Microwave Conference (GeMiC), Freiburg, 2018, pp. 343-346.

[12] Yishay R B, Elad D. D-band Dicke-radiometer in 90 nm SiGe BiCMOS technology[C]. 2017 IEEE MTT-S International Microwave Symposium (IMS), Honololu, HI, 2017, pp. 1957-1960.

[13] LIU Jun, LV Xin, YU Wei-Hua, *et al*. Design and realization of D-band InP MMIC amplifier with high-gain and low-noise[J]. *Journal of Infrared & Millimeter Waves*(刘军,吕昕,于伟华,等.D波段InP基高增益低噪声放大芯片的设计与实现.**红外与毫米波学报**), 2019, **38**(2): 144-148.

[14] ZHANG Jian-Jun, ZHOU Jing-Tao, YANG Cheng-Yue, *et al*. A 270 GHz high performance waveguide detector utilizing a zero-bias Schottky diode[J]. *Journal of Infrared & Millimeter Waves*(张建军,周静涛,杨成樾,等.基于零偏置肖特基二极管的270 GHz高性能波导检波器.**红外与毫米波学报**),2015,**34**(1):1-5.